Automatic and Unsupervised Water Body Extraction Based on Spectral-Spatial Features Using GF-1 Satellite Imagery

Yongjun Zhang, Xinyi Liu, Yi Zhang, Xiao Ling, and Xu Huang

***Abstract*— Water body extraction from remote sensing imagery is an essential and nontrivial issue due to the complexity of the spectral characteristics of various kinds of water bodies and the redundant background information. An automatic multifeature water body extraction (MFWE) method integrating spectral and spatial features is proposed in this letter for water body extraction from GF-1 multispectral imagery in an unsupervised way. This letter first discusses a spatial feature index, called the pixel region index (PRI), to describe the smoothness in a local area surrounding a pixel. PRI is advantageous for assisting the normalized difference water index (NDWI) in detecting major water bodies, especially in urban areas. On the other hand, part of the water pixels near the borders may not be included in major water bodies, *k*-means clustering is subsequently conducted to cluster all the water pixels into the same group as a guide map. Finally, the major water bodies and the guide map are merged to obtain the final water mask. Our experimental results demonstrate that accurate water masks were achieved for all seven GF-1 imagery scenes examined. Three images with a complex background and water conditions were used to quantitatively compare the proposed method to NDWI thresholding and support vector machine classification, which verified the higher accuracy and effectiveness of the proposed method.**

***Index Terms*— GF-1 imagery, image classification, spectral-spatial feature, water body extraction.**

I. Introduction

SURFACE waters, such as oceans, lakes, rivers, streams, and reservoirs, are vitally important for both the ecosystem and socioeconomic development; and accurate mapping of surface water is, therefore, essential for various hydrological research activities and for water source management, flood surveillance, and policy construction applications. Unfortunately, traditional surveying methods like *in situ* investigation are often time-consuming and cost-prohibitive for this purpose. Satellite remote sensing imagery is of increasing interest as a plausible alternative for delineating surface water efficiently. Due to the complexity of the atmospheric environment, background, and water quality, it is, therefore, imperative to investigate the automatic extraction of water bodies from remote sensing imagery.

A series of water body extraction approaches has been proposed to date, which can be divided into the following three categories.

1) *Spectral Features:* The normalized difference water index (NDWI) [1] is frequently used in water body extraction. In some applications, the modified NDWI [2] is used since NDWI has been proven to fail in some of the built-up scenes. More complex water indexes [3]–[5] have been proposed in recent years to compensate for this shortcoming, which either have specific requirements for bands like middle infrared or introduce higher computational complexity compared to NDWI.
2) *Spatial Features:* The different reflection properties of spectral features, which are caused by water pollution and confusion with similar objects, such as dark buildings and shadows, make them unsuitable for water body mapping from satellite imagery. Thus, the neighborhood features of the pixels are applied to extract water bodies from remote sensing imagery, such as texture [6], morphological profiles [7], homogeneity [8], and so on.
3) *Spectral-Spatial Features:* Techniques in this category integrate both spectral features and spatial features in one framework [9], [10]. However, a proper combination strategy is essential to avoid information loss or imprecise classification.

Increasingly, more water body extraction algorithms based on deep learning have been proposed in the literature in recent years and rather high accuracy has been reported in most cases [11]–[13]. However, these algorithms have not been widely used in practical applications, mainly because of their strict requirements: 1) a considerable number of training samples to handle the complexity of various kinds of water bodies and it is costly to build such data set [12] and 2) high-performance professional graphics cards and redundant time to accomplish the training.

Based on the aforementioned past research, this letter discusses the following two common issues in water mapping and remedies for them.

1) Although NDWI is a common and efficient method in water mapping for multispectral remote sensing imagery, it fails to distinguish water and built-up lands, leading to false water extraction results in urban areas. This letter,

Manuscript received October 7, 2018; accepted December 10, 2018. Date of publication December 28, 2018; date of current version May 21, 2019. This work was supported in part by the National Key Research and Development Program of China under Grant 2018YFB0505003, and in part by the National Natural Science Foundation of China under Grant 41571434, Grant 41322010, and Grant 41701540. *(Corresponding author: Yongjun Zhang.)*

Y. Zhang and X. Liu are with the School of Remote Sensing and Information Engineering, Wuhan University, Wuhan 430072, China (e-mail: zhangyj@whu.edu.cn).

Y. Zhang is with the Shanghai World Financial Center, Morgan Stanley, Shanghai 200120, China.

X. Ling is with the Future Cities Laboratory, Singapore-ETH Centre, Singapore 138602.

X. Huang is with the Engineering Developing, Wuhan Engineering Science and Technology Institute, Wuhan 430019, China.

Color versions of one or more of the figures in this letter are available online at http://ieeexplore.ieee.org.

Digital Object Identifier 10.1109/LGRS.2018.2886422

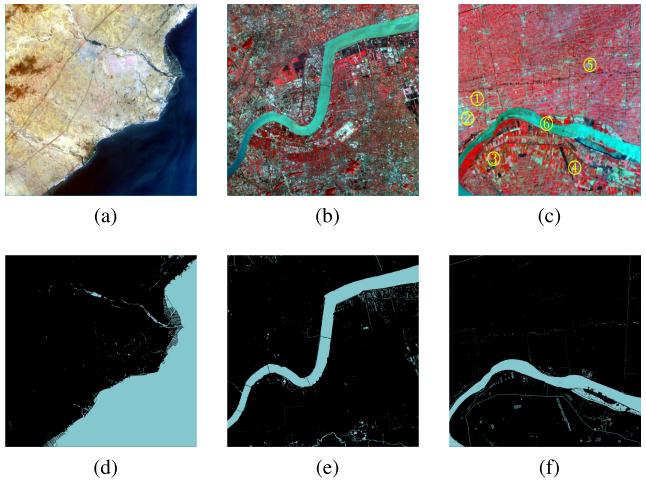

Fig. 1. Experiment images and their corresponding references. (a) Bohai. (b) Qiantang River. (c) Yangtze River. (d)–(f) Reference maps of (a)–(c), respectively. (Top) Color infrared composites of experiment image $1 \sim 3$, with R = NIR band, G = red band, and B = green band. (Bottom) Corresponding references. Bright color: water.

therefore, proposes the pixel region index (PRI) which describes the smoothness around the central pixel to assist NDWI to rule out build-up pixels.

2) Removal of the border pixels from water extraction results is essential for improving the mapping accuracy.

Most water extraction methods only depend on spectral features, which can cause disconnection and noises along the water border due to complex intensity variations. Spatial features (e.g., morphological profiles), if applied to optimize the results, always yield a reduction in the mapping accuracy. To overcome these difficulties, this letter explains how to remove the pixels with quite low-PRI features, which are considered as suspected border pixels, and then a method similar to region growing is applied to achieve water body extraction with high accuracy and continuity.

II. Study Object and Experimental Data Sets

A. Introduction of GF-1 Multispectral Imagery

Our research focuses on the GF-1 satellite, the first satellite of the Chinese High-Resolution Earth Observation System. Two multispectral cameras of 8-m resolution with a 4-day revisiting cycle are mounted on the GF-1 satellite, and the image extent of each camera is about 4500×4500 pixels. Thus, it has the characteristic of a relatively high spatial resolution and a short revisiting cycle at the same time. In addition, the multispectral bands of this imagery consist of blue ($0.45 \sim 0.52 \mu$m), green ($0.52 \sim 0.59$ μm), red ($0.63 \sim 0.69$ μm), and near infrared (NIR) ($0.77 \sim 0.89$ μm) bands.

B. Data Sets

Three GF-1 multispectral images were used for our quantitative comparison (Fig. 1) with the reference to these three images depicted manually with the help of Google Earth.

Experiment image 1, as shown in Fig. 1(a), contains the sea border of the Bohai Sea at Suizhong County, Liaoning Province, China, with a longitude range of 120.0874°–120.5829° and a latitude range of 40.0612°–40.4397°. The main water body types are broad and blue with darker pixels at the middle bottom of this image, and some small blue water areas distributed in the middle and top parts of the image. The background types in this image are mostly bare soil, bright build-ups, and dark mountain areas.

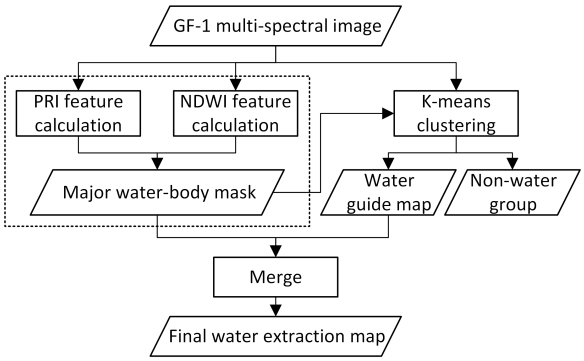

Fig. 2. Workflow of the proposed method.

Experiment image 2, as shown in Fig. 1(b), contains a part of the Qiantang River at Hangzhou City, Zhejiang Province, China, with a longitude range of 120.1701°–120.6267° and a latitude range of 30.1023°–30.4952°. There are six large water bodies, shown as blue in the left part and green in the right part in the pseudocolor image, which indicates the spectral changes of the water bodies. Small water fragments are also distributed in the whole image. Both bright and dark water bodies are recognizable in this image. This scene is in an urban area that contains bright and dark build-ups, vegetation, and bare soil.

Experiment image 3, as shown in Fig. 1(c), contains the downstream of the Yangtze River near the estuary of the Yellow Sea, with a longitude range of 121.1542°–121.5982° and a latitude range of 31.7035°–32.0675°. The main water body is a part of the Yangtze River, which is quite turbid. Sediments are apparent in the middle of the river. Small water bodies along the river reflect different chromatic characteristics compared to the largest water body. Build-ups and vegetation are the principal background types.

III. Methodology

The proposed method includes three stages.

1) Spatial and spectral features, PRI and NDWI, respectively, are integrated in order to obtain the major water body mask.
2) K-means clustering is employed to cluster the pixels into different groups based on their internal properties, which then are further classified into either a water group or a nonwater group with the guidance of the major water body mask obtained in the previous stage. The water group is called the water guide map for its effect in the next stage.
3) The major water body mask and the water guide map are merged to obtain the final water extraction map.

The overall flowchart of the proposed method is shown in Fig. 2. It is worthy to note that the input of this method is the GF-1 radiometric corrected multispectral image. Thus, no radiometric correction steps are conducted.

A. Pixel Region Index

Huang [14], [15] proposed a pixel shape index (PSI) and the extended structural feature set (SFS) to examine the context

of each pixel and measure the spatial dimensions of groups of spectrally similar connected pixels. PSI and SFS compute the direction lines histogram (DLH) for each pixel to describe the shape of the object to which the pixel belongs. This property is advantageous for differentiating pixels of different classes with similar spectral features but distinct spatial features. However, water bodies have various spatial features so, the sensitivity of PSI and SFS to spatial differences would decrease the accuracy of mapping water bodies to some extent. PRI is designed to overcome this kind of weakness in water body extraction and reflects the smoothness of a water body.

Given pixel p, the PRI value is defined as the area (number of pixels) of similar spectral pixels surrounding the pixel based on region growing, pseudocode of which is displayed in Algorithm 1.

Algorithm 1: PRI Calculation of Pixel p

Input : pixel p, a homogeneity threshold T_1, an area threshold T_2.
Output: The PRI value of pixel p.

Add $p \rightarrow region$
for *each* $P \in region$ **do**
  for *each pixel* $p' \in Neighborhood(P)$ *and* $Status(p') \neq VISITED$ **do**
    if $Homogeneity(p, p') < T_1$ *and* $\sharp region < T_2$ **then**
      Add $p' \rightarrow region$
      $Status(p') = VISITED$
    end
  end
end
return $PRI(p) = \sharp region.$

The homogeneity of each surrounding pixel p' with respect to the given pixel p is formulated as

$$\text{Homogeneity}(p, p') = \sum_{i=1}^{n} |p_i - p_i'| \tag{1}$$

where n denotes the number of bands, and p_i and p_i' represent the spectral value for band i of the given pixel p and the neighboring pixel p', respectively.

Three aspects should be noted.

1) Different from PSI and SFS, which are based on DLH, PRI does not include direction information and the homogenous surrounding pixels are taken into consideration without distinction. Therefore, pixels belonging to the same object with different orientations have a uniform feature value theoretically. As shown in Fig. 3, all types of water bodies have larger PRI values than other common materials, while their DLHs are quite different.
2) Water bodies, in general, are smoother than background objects. Thus, they tend to have larger PRI values, which are a valuable feature in separating water pixels from build-up pixels. An example of PRI and NDWI features for six classes in a GF-1 multispectral image is shown in Fig. 3. It can be seen that vastly different PRI values are achieved between water bodies (pool and river) and build-ups (road and building), all of which have positive NDWI values.

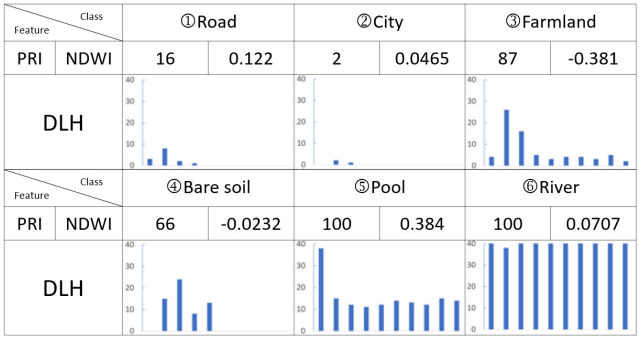

Fig. 3. PRI, NDWI, and DLH features for six classes from a GF-1 multispectral image [Fig. 1(c)]. The PRI parameters used in this figure are $T_1 = 40$, $T_2 = 100$. Some of the water types have similar large PRI values but various DLHs. Both water bodies and build-ups have positive NDWI values but different PRI values.

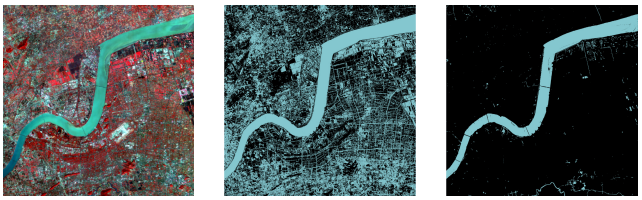

(a) (b) (c)

Fig. 4. (a) Experiment image 2. (b) NDWI map thresholded by peaks-valley method, lots of build-ups are retained. (c) Major water body mask obtained by the proposed method, almost all build-ups are removed.

3) Unlike region growing which checks the similarity of the seed pixels and its nearest neighbor, homogeneity in PRI is always measured between the given pixel and its surrounding pixels. It is better to reflect the smoothness around the given pixel.

B. Major Water Body Mask by Integration of PRI and NDWI Features

The smaller the water bodies are, the larger the positive NDWI value tends to be, which is caused by dissolved sediments. However, build-up land also has small and positive NDWI values so, it is impossible to distinguish large water bodies and build-up land only by NDWI. To address this problem, the PRI feature is added to assist in detecting water bodies (see Fig. 4); and this stage is divided into the following steps.

1) Classify the pixels according to the PRI feature

$$\begin{cases} C_{\text{large}}, & T_2 \leq \text{PRI}(p) \\ C_{\text{small}}, & T_3 \leq \text{PRI}(p) < T_2 \\ \text{discarded}, & \text{Otherwise} \end{cases} \tag{2}$$

where C_{large} and C_{small} represent large and small PRI feature class, respectively.
2) Compute the NDWI of each pixel in C_{large}, and apply the peaks-valley method on the histogram of the NDWI to mark out the water pixels, which are then grouped into objects as large water bodies. Similar process is conducted to C_{small} to obtain the small water bodies.
3) Combine large water bodies and small water bodies to obtain the major water body mask.

The PRI reflects the smoothness and the size of the object to which the targeted pixel belongs and is applied to detect large water bodies and rule out rather small objects at this stage.

C. Water Guide Map Using K-Means Clustering

Some water pixels near the border of water bodies may be neglected in Section III-B, since these pixels have lower PRI values due to mixed border pixels. To deal with this situation, one may use region growing method with the major water body mask (see Section III-B) taken as seed points set. However, this will lead to a new problem: how to determine a homogeneity threshold suitable for various water bodies. To circumvent this problem, k-means clustering is used to recover such water borders by considering all the spectral bands.

It is of great importance that before grouping pixels into objects in the k-means clusters, all the pixels having low PRI values (not larger than T_3) should be removed because pixels with low PRI values are quite different from their neighborhood and, thus, should be labeled with a different classification. Otherwise, the global spectral information used in k-means would neglect such local spatial information, which would lead to mixed water and background pixels at the borders.

The cluster number is given by a fixed number, i.e., 10 in this letter. Therefore, water pixels with similar spectral characteristics are clustered into the same group. Due to the different spectral properties of water pixels, several clusters are generated, all of which represent water bodies. The major water body mask is used to guide the potential type of clusters. If more than 10% of the pixels in a group are classified as water pixels in the water mask, the cluster is considered a candidate water class. Finally, a guide map is generated, which consists of different clusters of potential water pixels.

D. Integration of the Major Water Body Mask and the Water Guide Map

The major water body mask contains almost all the water pixels except for those near the water border, while the water guide map also contains those water pixels but is mixed with nonwater pixels, thereby taking the advantages of both to obtain the final water mask at this stage.

For each water body in the major water body mask, similar to region growing, all the pixels are considered as seed points. For every seed point, the process is as follows.

1) The seed point is skipped if all the nearest neighborhoods are also seed points or are not in the guide map;
2) The nearest neighborhoods of the seed point, which are in the guide map, are marked as seed points, to which the process is applied again.

When the process is completed for all the seed points, the entire water body is obtained as well as the final water extraction map.

IV. Experiments

A. Comparison Methods

The proposed method was quantitatively compared with three other methods, i.e., OTSU thresholding on NDWI (NDWI-OTSU), support vector machine–spectral (SVM-S), and support vector machine–co-occurrence (SVM-C). NDWI-OTSU applies histogram segmentation on the NDWI feature of the given image whereby the pixels having higher values than the OTSU threshold is classified as water [5]. SVM-S uses the spectral bands as input features [16]. SVM-C uses the spectral bands and the angular second moment (ASM) [17] of the gray-level cooccurrence matrix as features. The number of training samples in SVM is 50 for water (including rivers, ponds, and lakes) and 50 for nonwater (including buildings, roads, farmlands, and bare soils), respectively. The kernel function used in SVM is a radial-based function, and parameters c and γ are chosen by grid researching with five-fold cross-validation to achieve the best results on the training samples.

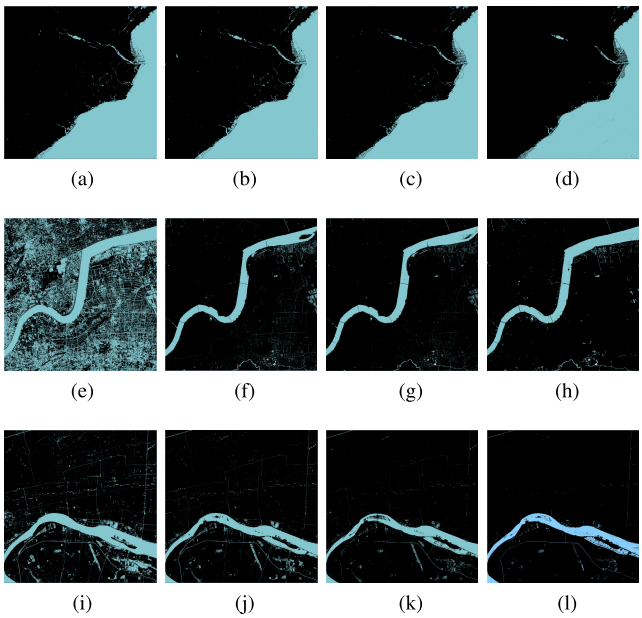

Fig. 5. Comparison of NDWI-OTSU, SVM-S, SVM-C, and MFWE. Bright color: water. (a) NDWI-OTSU. (b) SVM-S. (c) SVM-C. (d) MFWE. (e) NDWI-OTSU. (f) SVM-S. (g) SVM-C. (h) MFWE. (i) NDWI-OTSU. (j) SVM-S. (k) SVM-C. (l) MFWE.

The accuracy assessment method was conducted by counting the pixels of the correct and incorrect classifications, followed by comparing the extracted pixelwise results with the reference maps [Fig. 1(d)–(f)]. Given NN-the pixels number, the confusion matrix represents four classes of consistency of the extraction results: true positive (TP), false positive (FP), true negative (TN), and false negative (FN). Then, the producers accuracy (PA), users accuracy (UA), overall accuracy (OA), and kappa coefficient (Kappa) measurements were calculated based on the statistics of TP, TN, FP, and FN. In general, $\mathrm{PA} = \mathrm{TP}/(\mathrm{TP}+\mathrm{FN})$ reflects an omission error and $\mathrm{UA} = \mathrm{TP}/(\mathrm{TP}+\mathrm{FP})$ implies a commission error [18].

B. Parameter Tuning

The thresholds of the proposed method defined by experience, $T_1 = 40, T_2 = 100$, and $T_3 = 5$, were applied to all the experiments. T_1 limits the homogeneity difference in PRI calculation and can be fixed with a tolerance range of 10 since the PRI value is distinct enough to stand out the water bodies. The spatial resolution of GF-1 multispectral imagery is 8 m, then a smooth surface which is not smaller than $T_2 \times 8^2$ m^2 $= 6400$ m^2 is, for the most part, believed to be water or farmlands and unlikely to be others (especially build-ups). The lower bound of area T_3 is set to 5 in this

TABLE I
QUANTITATE COMPARISON OF NDWI-OTSU, SVM-C, SVM-S, AND MFWE

Method	Types	Experiment image 1				Experiment image 2				Experiment image 3			
		PA(%)	UA(%)	OA(%)	kappa	PA(%)	UA(%)	OA(%)	kappa	PA(%)	UA(%)	OA(%)	kappa
NDWI-OTSU	Water	**99.90**	96.84	98.98	0.9887	**99.94**	19.99	61.21	0.4930	**99.96**	58.26	94.61	0.9452
	Background	98.59	**99.96**			57.05	**99.99**			94.17	**99.99**		
SVM-S	Water	99.87	96.65	98.91	0.9879	83.51	82.88	96.73	0.9670	95.88	80.48	97.94	0.9792
	Background	98.49	99.94			98.15	98.23			98.11	99.66		
SVM-C	Water	99.67	98.08	99.31	0.9924	82.63	90.98	97.52	0.9750	86.68	91.44	98.39	0.9838
	Background	99.15	99.86			99.12	98.15			99.34	98.92		
MFWE	Water	99.38	**99.10**	**99.47**	**0.9942**	95.77	**99.18**	**99.51**	**0.9951**	86.71	**99.75**	**98.98**	**0.9898**
	Background	**99.61**	99.73			**99.91**	99.55			**99.98**	98.93		

letter since an area not larger than 5 pixels is more likely to be noise or border pixels rather than water body pixels.

C. Quantitative Comparisons

The water extraction maps (Fig. 5) and the quantitative results (Table I) of our comparison of the proposed method to three existing methods are discussed in this section. The PRI feature was shown to be of great benefit to NDWI in removing built-up land [Fig. 5(e)–(h)], and the proposed method achieved the best accuracy on all three images, which also had the best producer's accuracy of background and best user's accuracy of water. Thus, the proposed method was found to have low commission errors and relatively low omission errors. In addition, NDWI-OTSU had the tendency toward low omission error and high commission errors. SVM-S and SVM-C both obtained good results, while SVM-S had slightly high commission error leading to high overall error. Thus, the additional texture, ASM, was utilized to improve water extraction results. However, the spatial feature used in the proposed method was shown to contribute to the identification of water bodies without excessive concentration on the differences within water pixels. Therefore, compared to NDWI-OTSU, SVM-C, and SVM-S, the proposed method obtained the best results on all three images as a whole.

V. CONCLUSION

An automatic and unsupervised water body extraction method, called the multifeature water body extraction (MFWE) method, was proposed in this letter, in which, PRI is used to reflect the local spatial feature of water pixels. Our theoretical analysis concluded that as a modification for water extraction, PRI is useful to denote the local smoothness of objects. Peaks-and-valley histogram segmentation on NDWI and k-means clustering are used to integrate the spectral features, which complement the fact that the methods based on PRI may neglect water pixels near the borders. Our experimental results imply that MFWE outperformed NDWI thresholding and SVM with or without texture features. In our future work, we will focus on analyzing the sensitivity of the thresholds to the final performance and self-adaptive strategies for parameter tuning.

REFERENCES

[1] S. K. McFeeters, "The use of the normalized difference water index (NDWI) in the delineation of open water features," *Int. J. Remote Sens.*, vol. 17, no. 7, pp. 1425–1432, 1996.

[2] H. Xu, "Modification of normalised difference water index (NDWI) to enhance open water features in remotely sensed imagery," *Int. J. Remote Sens.*, vol. 27, no. 14, pp. 3025–3033, 2006.

[3] G. Zhang, G. Zheng, Y. Gao, Y. Xiang, Y. Lei, and J. Li, "Automated water classification in the tibetan plateau using Chinese GF-1 WFV data," *Photogramm. Eng. Remote Sens.*, vol. 83, no. 7, pp. 33–43, 2017.

[4] Q. Guo, R. Pu, J. Li, and J. Cheng, "A weighted normalized difference water index for water extraction using Landsat imagery," *Int. J. Remote Sens.*, vol. 38, no. 19, pp. 5430–5445, 2017.

[5] H. Xie, X. Luo, X. Xu, H. Pan, and X. Tong, "Evaluation of Landsat 8 OLI imagery for unsupervised inland water extraction," *Int. J. Remote Sens.*, vol. 37, no. 8, pp. 1826–1844, 2016.

[6] A. Essa, P. Sidike, and V. Asari, "Volumetric directional pattern for spatial feature extraction in hyperspectral imagery," *IEEE Geosci. Remote Sens. Lett.*, vol. 14, no. 7, pp. 1056–1060, Jul. 2017.

[7] M. Imani and H. Ghassemian, "Discriminant analysis in morphological feature space for high-dimensional image spatial–spectral classification," *J. Appl. Remote Sens.*, vol. 12, no. 1, p. 016024, 2018.

[8] R. Qin, "A mean shift vector-based shape feature for classification of high spatial resolution remotely sensed imagery," *IEEE J. Sel. Topics Appl. Earth Observat. Remote Sens.*, vol. 8, no. 5, pp. 1974–1985, May 2015.

[9] M. Fauvel, Y. Tarabalka, J. A. Benediktsson, J. Chanussot, and J. C. Tilton, "Advances in spectral-spatial classification of hyperspectral images," *Proc. IEEE*, vol. 101, no. 3, pp. 652–675, Mar. 2013.

[10] X. Huang, C. Xie, X. Fang, and L. Zhang, "Combining pixel- and object-based machine learning for identification of water-body types from urban high-resolution remote-sensing imagery," *IEEE J. Sel. Topics Appl. Earth Observ. Remote Sens.*, vol. 8, no. 5, pp. 2097–2110, May 2015.

[11] W. Zhao and S. Du, "Spectral–spatial feature extraction for hyperspectral image classification: A dimension reduction and deep learning approach," *IEEE Trans. Geosci. Remote Sens.*, vol. 54, no. 8, pp. 4544–4554, Aug. 2016.

[12] F. Isikdogan, A. C. Bovik, and P. Passalacqua, "Surface water mapping by deep learning," *IEEE J. Sel. Topics Appl. Earth Observ. Remote Sens.*, vol. 10, no. 11, pp. 4909–4918, Nov. 2017.

[13] Y. Chen, R. Fan, X. Yang, J. Wang, and A. Latif, "Extraction of urban water bodies from high-resolution remote-sensing imagery using deep learning," *Water*, vol. 10, no. 5, p. 585, 2018.

[14] X. Huang, L. Zhang, and P. Li, "Classification and extraction of spatial features in urban areas using high-resolution multispectral imagery," *IEEE Geosci. Remote Sens. Lett.*, vol. 4, no. 2, pp. 260–264, Apr. 2007.

[15] X. Huang, Q. Lu, and L. Zhang, "A multi-index learning approach for classification of high-resolution remotely sensed images over urban areas," *ISPRS J. Photogramm. Remote Sens.*, vol. 90, no. 11, pp. 36–48, 2014.

[16] G. Sarp and M. Ozcelik, "Water body extraction and change detection using time series: A case study of lake Burdur, turkey," *J. Taibah Univ. Sci.*, vol. 11, no. 3, pp. 381–391, 2017.

[17] N. Liu, C. Lu, M. Zhang, Z. Cui, Z. Cao, and R. Min, "Geospatial object partition based on angular second moment kernel," in *Proc. Int. Conf. Commun., Signal Process., Syst.* Singapore: Springer, 2017, pp. 464–471.

[18] Y. Zhou, J. Luo, Z. Shen, X. Hu, and H. Yang, "Multiscale water body extraction in urban environments from satellite images," *IEEE J. Sel. Topics Appl. Earth Observat. Remote Sens.*, vol. 7, no. 10, pp. 4301–4312, Oct. 2014.